Highly-Sensitive Unbalanced MZI Gas Sensor Assisted With a Temperature-Reference Ring Resonator

Ayat M. Taha ⓘ, Soha Yousuf ⓘ, Marcus S. Dahlem ⓘ, *Senior Member, IEEE*, and Jaime Viegas ⓘ, *Member, IEEE*

Abstract—**In this paper we study the gas sensing performance of a compact silicon photonics Mach-Zehnder interferometer (MZI) with a coiled sensing arm. A partially exposed sensor was fabricated using deep UV lithography, with a process resolution of 248 nm. Testing with inert gases, He and N_2, resulted in a measured sensitivity and limit of detection of ~1458 nm/RIU and ~8.5×10^{-5} RIU, respectively, in a sensing volume of 1.852 picoliters. The temperature sensitivity of the sensor was 166 pm/°C and the inclusion of a cladded ring-resonator, post-MZI, allowed resolving the temperature drift due to gas flow. In order to further enhance the overlap of the optical mode with the measurand and thus the sensitivity, a suspended MZI was designed and simulated with an expected sensitivity of ~5500 nm/RIU, for wavelengths around 1550 nm and a temperature of 300 K.**

Index Terms—**Mach-Zehnder interferometer, ring resonator, silicon-on-insulator, silicon photonics.**

I. INTRODUCTION

INTEGRATED optical devices are becoming increasingly attractive in the field of optical sensing, particularly in environmental, chemical and biochemical detection. Their advantages such as high sensitivity, integrability with electronic devices, compactness, and low cost, makes them well suited for optical sensing applications [1], [2], [3], [4], [5]. The most common sensing mechanism is based on the change of the optical mode's effective index due to variation of the bulk solution's refractive index, as a result of the overlap between the evanescent field of the guided mode and the measurand [6], [7]. Therefore, the concentration of the measurand is proportional to the magnitude of the change in effective refractive index of the propagating optical mode. Waveguide sensors built on a silicon-on-insulator

Ayat M. Taha and Jaime Viegas are with the Electrical Engineering and Computer Science Department, Khalifa University, Abu Dhabi 127788, UAE (e-mail: ayat.taha@ku.ac.ae; jaime.viegas@ku.ac.ae).

Soha Yousuf was with the Electrical Engineering and Computer Science Department, Khalifa University, Abu Dhabi 127788, UAE. She is now with the Smart Materials Lab (SML), Division of Science and Mathematics, New York University Abu Dhabi, Abu Dhabi 129188, UAE (e-mail: sohaekrima@gmail.com).

Marcus S. Dahlem was with the Electrical Engineering and Computer Science Department, Khalifa University, Abu Dhabi 127788, UAE. He is now with the IMEC, 3001 Leuven, Belgium (e-mail: Marcus.Dahlem@imec.be).

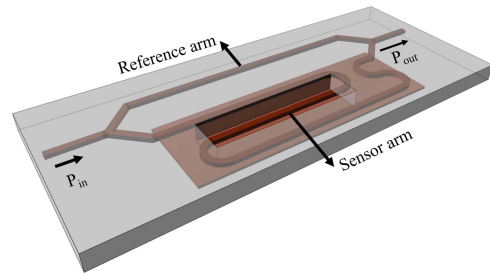Digital Object Identifier 10.1109/JPHOT.2022.3215713

Fig. 1. Illustration of a basic MZI sensor. The sensor consists of an input waveguide, a y-splitter leading into two arms, a y-combiner and an output waveguide. One arm is used as a reference and the other is used as a sensing arm. The waveguide of the sensing arm is exposed in order to interact with the measurand, while the reference arm is completely shielded from any perturbations by being covered by an oxide layer.

(SOI) platform demonstrate enhanced sensitivity due to the high-index contrast between the silicon and the dielectric cladding. The high-index contrast feature maximizes the sensitivity of the waveguides to very small changes in the cladding's refractive index, an effect especially prominent when using the transverse magnetic (TM) mode, in contrast with the transverse electric (TE) mode [8]. Integrated photonic sensors that use microring resonators or interferometric structures like Mach-Zehnder interferometers (MZI), are among the most used types of refractive index sensors [9], [10], [11], [12]. The performance of such sensors depend on several parameters, such as the operating wavelength, as well as physical dimensions including the radius of the microring resonator, the gap between the microring and the bus waveguide, the dimensions and the configuration of the waveguide, and the length of the arms of the MZI [1].

In particular, Mach-Zehnder interferometers are commonly favored as sensors due to their simplicity, high sensitivity, and low cost [1]. MZI sensors have been fabricated using different configurations including liquid-core waveguides [13], slot waveguides [14], and rib waveguides [15]. A basic schematic of an MZI sensor is shown in Fig. 1. High device sensitivity can be achieved by considerably increasing the length of the sensing arm of the MZI sensor. However, very long MZIs make them less suited for on-chip integration due to large footprint [16].

For instance, for the detection of a change in the refractive index on the order of 10^{-6}, a sensing arm of several mm in length is necessary [17]. In this paper, we present a 1-cm long partially exposed MZI on a 90 nm slab that was designed and
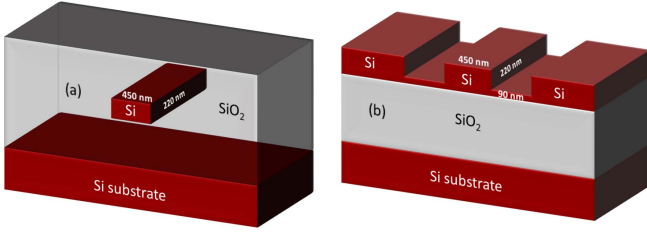
Fig. 2. Schematic representation of the proposed partially exposed MZI sensor: (a) cross-section of the reference arm; and (b) cross-section of the partially exposed MZI sensor arm.
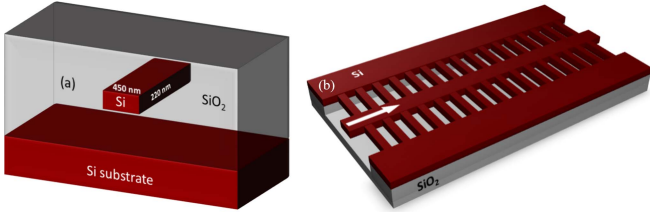

Fig. 3. Schematic representation of the proposed suspended MZI sensor: (a) cross-section of the reference arm; and (b) cross-section of the suspended MZI sensor arm.

fabricated for gas sensing applications. A schematic diagram of the reference arm and the sensor arm configuration is shown in Fig. 2. A suspended MZI sensor with sidewall gratings was also designed and demonstrated, the schematic diagram of the reference arm and the sensor arm configuration is shown in Fig. 3. The MZI sensors are assisted with a ring resonator, which is placed at their output, to detect the undesired temperature drift that results during sensing experiments. The sensing principle is based on evanescent field sensing where the field interacts with the measurand and induces a change in the effective refractive index of the optical mode. The change induced in the sensing arm of the MZI causes a phase shift, which varies with the concentration of the measurand [18]. In the following section, we describe the design and operating principle of the proposed MZI structures. Section III briefly discusses the analytical approximation to quantify the sensitivity of the MZI sensors and the performance limitations of the device. The fabrication method, optical setup, and optical characterization of the proposed MZI structures will be presented in Section IV. A gas sensing experiment conducted with the proposed partially exposed MZI sensor structure is presented in Section V. Finally, Section VI concludes and summarizes the sensors performance.

II. DESIGN AND OPERATING PRINCIPLE

The design parameters of the sensors were chosen such that a single-mode condition is fulfilled. The waveguides are designed on an SOI platform, consisting of a silicon core and a silica-based cladding. The reference arm of the partially exposed and suspended MZI sensors is a rectangular waveguide completely covered with silicon dioxide to avoid any perturbations from the measurand. The height of the reference waveguide core is set to be 220 nm and the width to be 450 nm. The operating wavelength is selected to be around 1550 nm, at which the

refractive index of silicon dioxide (SiO_2) and silicon (Si) is 1.444 and 3.476, respectively. The sensing arm of the partially exposed MZI sensor is a rib waveguide with a total height of 220 nm and a 450 nm-wide channel, patterned on a 90 nm-thick silicon slab, as shown in Fig. 2(b). The sensor was specifically optimized for TE mode operation, and is unbalanced in terms of the optical path length of the two arms. The sensor arm of the suspended MZI (silicon oxide cladding is removed from the top and the bottom) is designed via the use of the segmented wave guiding technique. The suspended arm is a 450 nm wide and 220 nm thick rectangular waveguide with sidewall gratings. The gratings act as the optical elements which bridge the suspended waveguide to a Si block, which is not released, for mechanical support as shown in Fig. 3(b). The period of the gratings is 400 nm (200 nm gap and 200 nm Si support). The sensor configuration performs best with TM-polarized light, given that TM mode eases the fabrication constraints of the gratings with period that satisfy the first-order Bragg condition, owing to its smaller effective refractive index relative to TE mode. The dimensions were carefully chosen such that, TM mode propagates with negligible propagation loss while enabling a further delocalized profile for achieving higher sensitivities. The length of the reference arm is set to be 750 μm while the sensor arm is set to be 850 μm long, hence, the suspended MZI is unbalanced with regard to the optical path length of each arm.

The operating principle of the MZI sensors can be stated as follows. The MZI transmission response is based on an interference pattern which corresponds to a phase shift between the light propagating in the two arms. This shift occurs by varying the path length of one of the arms, or due to different propagation constants in both arms. When the phase difference between the reference and sensing arms is a multiple of 2π radians, complete constructive interference occurs, resulting in maximum intensity [19]. The sensitivity of the MZI sensor, which is determined by the wavelength shift, caused by a variation in the effective refractive index at the sensing arm, is expressed as [20]:

$$\Delta\lambda = \lambda \frac{L_{sen}\Delta n_{eff_{sen}}}{L_{sen}n_{g_{sen}} - L_{ref}n_{g_{ref}}},\qquad(1)$$

where $\Delta n_{eff_{sen}}$ is the change in the effective index in the sensing arm, $n_{g_{sen}}$ and $n_{g_{ref}}$ are the group indices of the sensing and reference arms, respectively. L_{ref} and L_{sen} are the lengths of the reference and sensing arms, respectively, and λ is the operating wavelength. It is apparent from (1) that for the same variation of the cladding refractive index, the sensitivity of an MZI sensor which works based on a wavelength shift, can be much higher than the sensitivity of a microring sensor, given by (2) [21], [22], if an appropriate ratio between the reference and the sensing arm is chosen so that the optical path length difference is very small [20]. The period of the MZI response is also determined solely by the optical path length difference as indicated in (3) [23]. Therefore, the length of the MZI arms have to be carefully selected in order to obtain an interferometric response with sufficient spectral spacing for optimal sensing performance and to allow for maximum dynamic range of detection.

$$\Delta\lambda = \lambda \frac{\Delta n_{eff_{sen}}}{n_{eff_{sen}}},\qquad(2)$$

where $\Delta\lambda$ is the measured resonance wavelength shift, λ is the operating wavelength, $n_{eff_{sen}}$ is the effective index in the sensing arm, and $\Delta n_{eff_{sen}}$ is the determined effective index shift caused by the change in temperature.

$$\Lambda = \frac{\lambda^2}{L_{sen} n_{g_{sen}} - L_{ref} n_{g_{ref}}} \,, \qquad (3)$$

where λ is the operating wavelength, $n_{g_{sen}}$ and $n_{g_{ref}}$ are the group indices of the sensing and reference arms, respectively, and L_{ref} and L_{sen} are the lengths of the reference and sensing arms, respectively.

The contrast of the interference signal depends on the splitting ratio of the y-splitter and on the propagation loss of the guided modes in each arm of the interferometer. The contrast is quantified by the fringe visibility, which we define here as the difference between the maximum and the minimum intensity levels of the interference signal. A high visibility is achieved if the splitting ratio is 3 dB and the propagation loss in the reference and sensing arms are the same [17]. In addition, a maximum output power is obtained if the MZI sensor is balanced (identical optical path lengths of the reference and sensing arms). However, in this case, the lengths of the two arms are not equal, and the intensity ratio in each arm depends on the splitter and combiner geometries. In this work the y-branch used on either side of the MZI sensor has a similar configuration as in [24].

III. Analytical Approximation and Performance Limitations

One fundamental limitation of an MZI sensor is the temperature dependence. This limiting factor can degrade the sensor performance due to the high thermo-optic (TO) coefficient of silicon ($\sim 1.86 \times 10^{-4}$ K^{-1}) [25]. There are several different ways in which the temperature sensitivity can be dealt with. Some solutions involve the use of materials that cancel out the effect of the high TO coefficient of silicon but are not compatible with CMOS processing, and some others require a large power consumption due to heating the sensor device to stabilize the temperature [26]. In [27], [28], [29], [30], athermal performance is attained by utilizing a surface layer (polymer cladding) of negative TO coefficient. However, using the polymer overlay cladding approach is not compatible with CMOS processes. Titania (TiO$_2$), that has a high negative TO coefficient is also another appealing CMOS-compatible approach in mitigating the TO effect [31], [32]. The temperature-dependent wavelength shift of a silicon MZI can be handled by careful design of the arm dimensions [23], [33]. Another approach involves setting a different polarization in each arm of the MZI device [34], or using waveguides with different material composition in order to balance the thermo-optic effect in each arm [35]. Most solutions work around obtaining a difference in the MZI arms (varying the configuration, polarization, etc.) such that an opposing temperature-dependent phase change is induced in each arm, thereby reducing the temperature-dependent wavelength shift of the MZI.

In this work, a ring resonator is placed at the end of the MZI sensors such that the output waveguide of the MZI acts as the through port of the ring resonator. In this manner, the detected output response incorporates the MZI interferometric response with the ring through port response. The ring resonator is buried in SiO$_2$ to avoid any undesired perturbations from the measurand. Therefore, any observed shift in the ring response is merely due to temperature variation resulting from the surrounding measurand. The temperature-reference ring resonator on the partially exposed sensor has the following parameters: 220 nm silicon layer thickness, a ring core width of 450 nm and a radius dimension of 10 μm. The coupling gap between the output waveguide and the ring resonator was set to be 300 nm, and the FSR was calculated to be around 9 nm for TE mode, at 1550 nm. A ring resonator is also used for the suspended MZI sensor to counterbalance the temperature influence. The temperature-reference ring resonator has the following parameters: 220 nm silicon layer thickness, a ring core width of 450 nm and a radius dimension 20 μm. The coupling gap between the output waveguide and the ring resonator was set to be 500 nm, and the FSR was calculated to be around 5 nm for TM mode, at 1550 nm. Calculating the ring's $n_{eff_{sen}}$ using Lumerical's Finite-Difference Eigenmode (FDE) solver, and recording the experimental induced temperature-dependent wavelength shift ($\Delta\lambda$), the effective index change ($\Delta n_{eff_{sen}}$) is then deduced using (2) for the buried ring resonator. Consequently, a set of FDE solver simulations were conducted to quantify the corresponding change in the refractive index of silicon (Δn_{Si}) that would prompt the induced $\Delta n_{eff_{sen}}$. As a result, having calculated the change in the refractive index of silicon, and using its TO coefficient (TOC$_{Si}$), the temperature drift (ΔT) resulting from the measurand can then be deduced as can be seen from (4). Determination of this temperature drift would assist in eliminating the temperature impact on the MZI sensor and thereby avoiding ambiguity in the sensor performance. This is a reliable approach in determining the temperature-dependent wavelength shift that results in the MZI sensor.

$$\Delta T = \frac{\Delta n_{Si}}{TOC_{Si}} \,, \qquad (4)$$

To evaluate the sensitivity of the proposed sensor structures, a partially exposed MZI was studied using FDE solver simulations and a Matlab script. This evaluation was performed using TE light with the aforementioned waveguide dimensions. The refractive index of the medium cladding was increased in increments from the refractive index of air ($\sim$1.00027 at 1550 nm) [36], to a refractive index of 1.00127 and the wavelength shift which is given by (1) was calculated for each case to determine the expected sensitivity value. Having calculated the wavelength shift for different cladding refractive index, the sensitivity of the exposed MZI, defined as the slope of the linear response obtained in Fig. 4, was approximately 2071 nm/RIU.

The simulation of the suspended sensor was conducted via the use of ports in Lumerical finite difference time domain (FDTD) along with Optical N-Port S-parameter (SPAR) element in INTERCONNECT. The length and the complexity of the suspended sensor, causes the otherwise numerically rigorous and accurate 3D FDTD simulations, to be computationally intensive and more time consuming. The S-parameters, as a function of
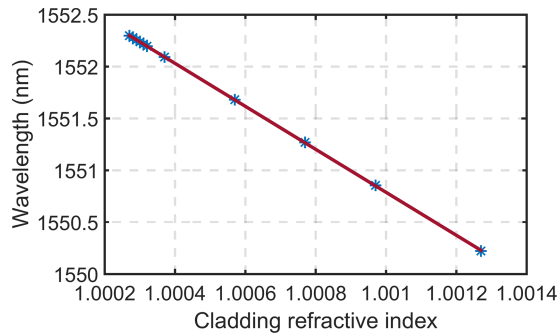
Fig. 4. Simulated wavelength shift for different cladding refractive index for the partially exposed MZI.
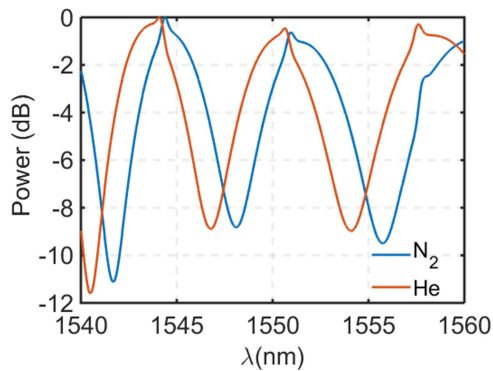

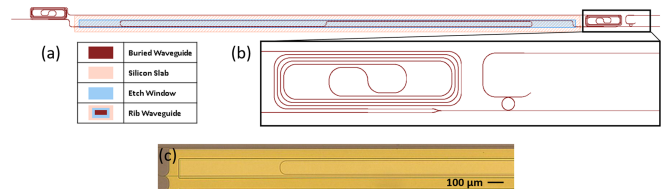Fig. 5. Simulated gas sensitivity for the suspended MZI.

Fig. 6. Illustration of the partially exposed 1-cm long MZI sensor on a 90 nm slab: (a) GDS layout of the MZI sensor; (b) zoom-in of the temperature-reference ring; and (c) top-view optical micrograph of the fabricated sensor arm.
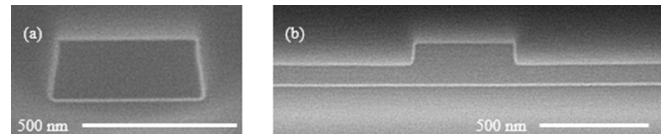

Fig. 7. SEM images of the fabricated partially exposed MZI sensor: (a) cross section view of the reference waveguide; and (b) cross-section of the rib arm.

wavelength, are then imported into INTERCONNECT, in which a compact model is used, so as to study the behavior and performance of the sensor. The ports were carefully positioned such that a total length of 50 μm, from the beginning of high to the end of low refractive index regions of the periodic grating structures, is attained. In this manner, the extracted S-parameters can be imported to a series of SPAR elements in INTERCONNECT, to complete the actual total length of the sensor arm, with higher simulation accuracy and significantly faster computation time. For the reference arm, MODE waveguide in INTERCONNECT is used in which wavelength dependent properties, among which are the effective and the group indices of the buried waveguide, can be directly imported from Lumerical MODE Solutions, resulting in accurate simulation results. The characteristic of the sensor was tested by an Optical network analyzer (ONA) element which is used for both, injecting light into the MZI and determining the response of the sensor as a function of wavelength. The 3D FDTD simulation of the 50 μm long device with ports was conducted in different gaseous medium: Helium (He), and Nitrogen (N_2), with the aim of computing the bulk sensitivity of the device. The simulation in INTERCONNECT was performed for both gases, the results of which are shown in Fig. 5. INTERCONNECT simulation results demonstrated that the response shifts towards a shorter wavelength when the cladding medium alters from N_2 to He gas. Sensitivity as high as 5500 nm/RIU, near 1550 nm wavelength, was observed, proving the potential of the suspended structure in sensing applications.

IV. DEVICE FABRICATION AND OPTICAL CHARACTERIZATION

The partially exposed MZI sensor was patterned using 248 nm deep UV lithography, in a silicon photonics processing line, in participation with A*STAR Institute of Microelectronics (IME)-Singapore. The optical test setup was comprised of a tunable laser source (Agilent 81600B) with an output wavelength ranging from 1460–1640 nm and a MATLAB script to sweep the laser wavelength for data acquisition. The time required to end the wavelength sweeping depends on various parameters such as: the wavelength range, number of scans, the sweeping speed of the source, and the resolution. A tapered lensed fiber with a focal spot size of 1.7 μm is used to couple light from the source to the waveguides and from the waveguides to the optical power sensor (Agilent 81636B). The output was imaged on a visible camera with a 20x microscope objective and an IR camera was used to view the light propagating along the waveguides.

The chip was firmly secured on a custom aluminum chuck using a vacuum pump and was moved freely in the X, Y and Z directions using the Thorlabs piezo controller. The fibers were also aligned using the Thorlabs controller and the light from the laser source is changed using a polarization controller (Agilent 8169 A) to any well-defined state of polarization. The MZI sensor layout and the optical micrograph of the exposed sensing region are shown in Fig. 6. The cross-sectional SEM image of the reference and rib waveguide, of the partially exposed MZI sensor arms is depicted in Fig. 7. The dimensions of the fabricated sensor arms exhibited a sidewall angle which was measured to be around 85 degrees.

The spectral response of the partially exposed MZI sensor is shown in Fig. 8. The FSR was measured to be ∼4.3 nm, which is in good agreement with the simulated FSR, and the difference between the maximum and the minimum intensity levels of the interference spectrum, which relates to the fringe visibility, was ∼22 dB. It is essential to obtain a high contrast interference fringe pattern, making it easy to track the position of the minimum of the spectrum, in order to accurately measure the sensitivity of an MZI sensor. The fringe visibility in the
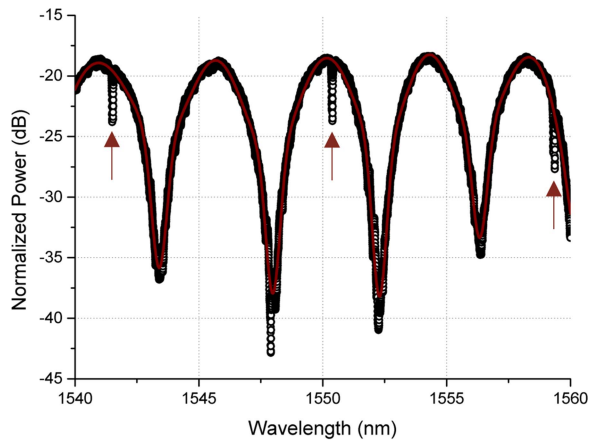
Fig. 8. TE mode transmission spectrum of an MZI with 90 nm slab partially exposed in air with a 450 nm waveguide width and an arm with a length of 1-cm (Fitting in solid red line). The arrows indicate the ring through port response.

Fig. 10. Gas chamber used to conduct the experiment: (a) the chamber is made of a polystyrene box with a lid on top, a gas inlet valve and two small openings on either side; one for the input fiber and one for the output fiber allowing easy access for optical characterization; and (b) zoom-in of the chip inside the gas chamber.
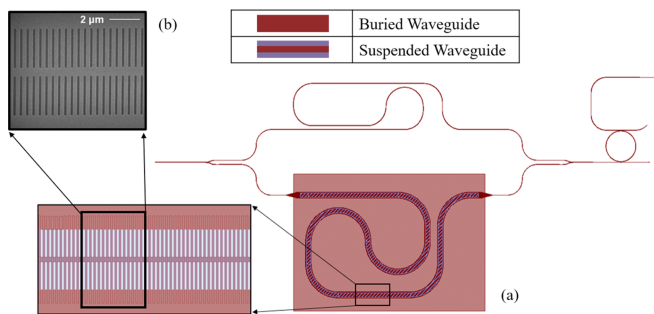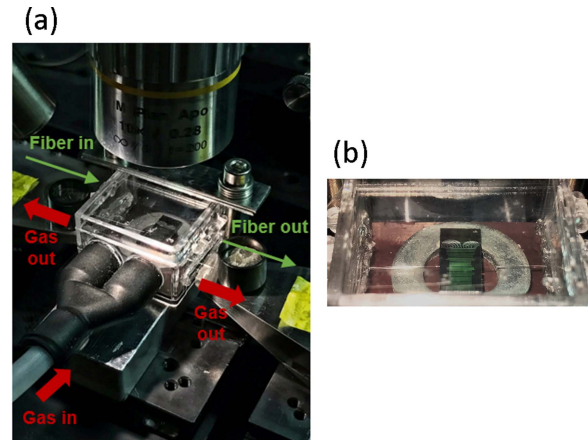

Fig. 9. Illustration of the suspended MZI sensor using sidewall gratings: (a) GDS layout of the MZI sensor with zoom-in-view of the suspended sensor arm; and (b) zoom-in SEM image of the gratings in the sensor arm.

partially exposed sensor is considerably high due to a balanced power and balanced splitting/loss ratio between the two arms. As mentioned earlier, the fringe visibility deteriorates when there is uneven power in the two MZI arms which could result from an uneven splitting ratio at the input coupler as well as different propagation losses in the two arms.

The suspended MZI sensor was fabricated by Applied Nanotools (ANT) using a 100 keV electron beam lithography system. Fig. 9 demonstrates the GDS layout design of the suspended MZI sensor and an SEM image of the fabricated suspended arm. However, the suspended MZI sensing performance was not possible to determine experimentally due to fabrication errors.

V. Sensing Experiment

A sensing experiment was conducted only for the partially exposed MZI sensor as the suspended sensor encountered various fabrication errors. Nevertheless, minimizing temperature drift is a crucial parameter to consider in a refractive index sensor design in order to quantify the sensitivity accurately, which as mentioned previously, will be achieved through the use of the ring resonator in the MZI design.

The response of the ring temperature sensor is shown in Fig. 8 with arrows. The MZI sensor and the ring resonator

were subjected to different temperature conditions by mounting the whole chip in a gas chamber and introducing two different gases alternatively: He and N_2. The gas chamber used in this experiment is shown in Fig. 10.

As a result of the gas change, a temperature drift led to a change in the core and the cladding refractive index, thereby changing the effective index of the ring resonator. A blue wavelength shift of around 36 pm was observed which indicates that the temperature dropped when the surrounding medium was changed from He to N_2 gas. Owing to helium's relatively lower molar mass, its average kinetic energy is larger and thus the temperature is higher [37]. Using the wavelength shift expression of the ring resonator (2), the change in the effective refractive index was calculated to be on the order of 10^{-5}. The ring's new effective index value was approximated by adding the original value of the effective index to the extracted $\Delta n_{eff_{sen}}$ i.e. ($n_{eff_{sen-new}} = n_{eff_{sen}} + \Delta n_{eff_{sen}}$). Having calculated the new effective index, the refractive index value of the Si core was deduced via FDE solver simulations as explained earlier, and subsequently, the refractive index change was extracted. Lastly, the TO coefficient of Si at 1550 nm was used to deduce the temperature drop which was found to be about 0.27 K.

Subsequent to calculating the temperature drop due to interchanging the gases, a similar analysis was carried out for the MZI sensor. FDE solver was used to calculate the field components and the effective index of the propagating mode in the reference and sensing arms. Several simulations were conducted to get wavelength sweeps for different temperatures and for both gases (He and N_2). The values of the obtained effective indices were then used in a Matlab script to detect the spectral shift (due to gas and temperature effects, and the gas effect alone (Fig. 11). The simulation results demonstrated that with taking into account the temperature effect, the sensitivity of the partially exposed MZI sensor decreased by 10.5%. Accordingly, the discrepancies in the spectrum wavelength shift due to unavoidable temperature
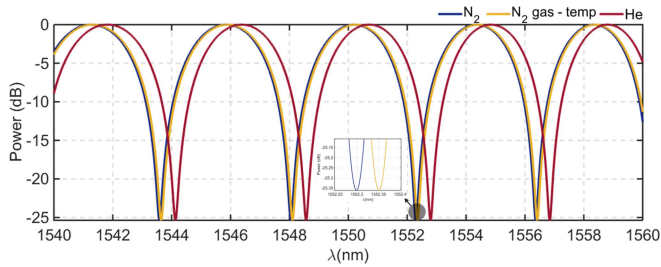
Fig. 11. Simulated gas and temperature sensitivity. The zoom-in plot demonstrates the shift of N_2 (blue line) to be due to changing the gas alone whereas the N_2 (yellow line) shift is due to the effect of both, changing the gas and the induced temperature drop (0.27 K calculated from the buried ring resonator).

Fig. 13. Resulting wavelength shift in the MZI sensor caused by interchanging gases from: (a) He to N_2, the response falls exponentially to a constant level with a time constant of 84 secs; and from (b) N_2 to He, the response rises exponentially with a time constant of 81 secs.
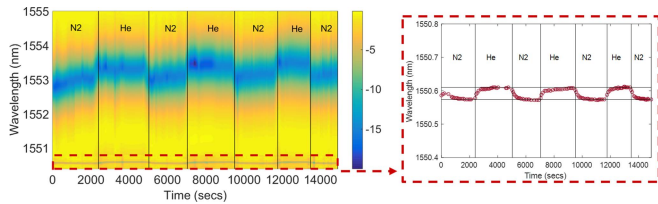

Fig. 12. Resulting transmission spectrum showing wavelength shift caused by interchanging the gases for the 1-cm long partially exposed MZI sensor. The color bar represents the output intensity in the dB scale. The 2D surface plot (left) shows how the MZI and the ring resonator sensors respond to two different surrounding mediums: Nitrogen and Helium gas. A total blue wavelength shift of around 350 pm results when the surrounding medium changes from He to N_2 gas for the MZI, and a wavelength shift of 36 pm (right plot) resulted for the ring due to temperature change.

change, can be calibrated for the MZI sensor via the use of the ring resonator.

The fabricated 1-cm long partially exposed MZI sensor was characterized in a gas sensing experiment alongside the ring using the gases: He and N_2, the results of which are shown in Fig. 12. The blue stripe indicates the transmission peak near 1552 nm and the color bar shows a 20 dB range used for plotting the optical power. A total blue wavelength shift of around 350 pm was observed for the MZI when the gas was switched from He to N_2, resulting in a measured sensitivity of around 1458 nm/RIU. A respected time of about 35 minutes was maintained between every transition, to fully replace the previous gas with the new gas by purging the chamber and to ensure stabilization. The switching of gases was repeated several times to check for reproducibility. When the surrounding gas alternates from He to N_2, the wavelength reduces exponentially with time and when the gas changes back to He, the wavelength increasing exponentially. The graph of the exponential function for each state of the MZI sensor is plotted in Fig. 13 with a time constant of 84 secs and 81 secs for the falling and rising exponential responses, respectively. The performance of the MZI gas sensor investigated in this work is summarized and compared with other optical gas sensors reported in the literature (Table I).

It is evident from the ring response that when the two gases were interchanged the temperature varied. Therefore, the measured sensitivity of the exposed MZI sensor is a result of both, the change in gases and the temperature simultaneously, which is one reason why the measured sensitivity is different from the
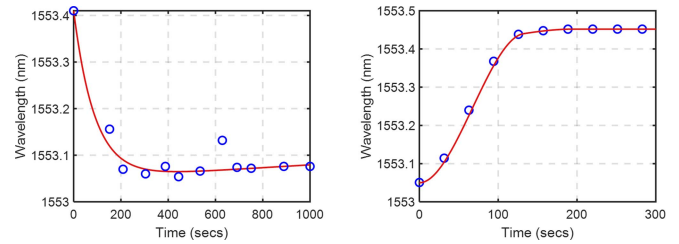
calculated sensitivity. Another potential reason for the difference is the sidewall angle of the fabricated waveguides, as seen in the cross-section image in Fig. 7, which varies along the length of the MZI sensor.

In order to address the aforementioned discrepancy with temperature, a temperature dependence experiment was conducted for both, the MZI and ring resonator sensors. The temperature characterization of the sensors was performed by tracking the wavelength shift while the temperature of the chip was raised from room temperature by about 10 °C. The experiment was conducted by placing the chip on top of a Peltier element and a thermocouple was mounted onto the chip's surface to accurately monitor the temperature. A voltage was applied to the Peltier element between every temperature point, necessitating a substantial waiting time for the temperature to stabilize and thus ensuring the thermal equilibrium of the thermocouple and the chip. The results of the temperature measurement is depicted in Fig. 14. Heating the chip has resulted in a spectral shift towards the longer wavelengths for the ring resonator, and a spectral shift towards the shorter wavelengths for the MZI sensor. The temperature-reference ring resonator exhibited a temperature sensitivity of 136 pm/°C, that agrees with the sensitivity deduced from the gas experiment which was ∼133 pm/°C. The MZI sensor on the other hand, reacts in an opposite manner to the ring resonator whereby increasing the temperature results in a negative slope of 166 pm/°C.

Fortunately, the MZI sensor demonstrates a low temperature dependence relative to the total sensitivity which was measured to be around 1458 nm/RIU. Having measured the temperature dependence of the MZI sensor and given that the temperature change occurring in the presence of the gases is known, it is now feasible to eliminate the temperature influence on the main sensor. Multiplying the previously calculated temperature drop (0.27 K) with the measured temperature sensitivity of the MZI sensor (166 pm/°C) results in a temperature-induced wavelength shift of around 44.82 pm. Removing the temperature-induced wavelength shift from the total measured wavelength shift of the sensor gives the gas-induced wavelength shift, which was found to be around 305.2 pm yielding a sensitivity of around 1272 nm/RIU. Therefore, as anticipated, eliminating the temperature effect from the MZI sensor reduces the sensitivity. In this case, the measured sensitivity was reduced by about 12.75%, which is in good agreement with the

TABLE I
COMPARATIVE TABLE OF STATE-OF THE-ART OPTICAL SENSORS FOR DIFFERENT GASES

| Sensor Type	Sensor Configuration	Gas	Bulk Sensitivity (nm/RIU)	Limit of Detection (RIU)	Reference
Photonic Crystal (PhC)	PhC air slot cavity	Nitrogen (N_2), Helium (He), Carbon-dioxide (CO_2)	510	1×10^{-5}	[38]
	Slot PhC	N_2, He, CO_2	421	1×10^{-5}	[39]
Microcavity	Optofluidic Fabry-Perot (FP) resonator	-	1053	5×10^{-4}	[40]
	Fiber FP cavity	Ethylene (C_2H_4), Methane (CH_4), He, CO_2	812.5	1.2×10^{-6}	[41]
Micro-ring Resonator	Grating double-slot micro-ring resonator	-	433.33	8.26×10^{-4}	[42]
	Slotted silicon micro-ring resonator	Acetylene	490	10^{-5}	[12]
MZI	Loop-terminated MZI	-	1070	3.6×10^{-3}	[43]
	Partially exposed MZI	He, N_2	1458	8.5×10^{-5}	This work
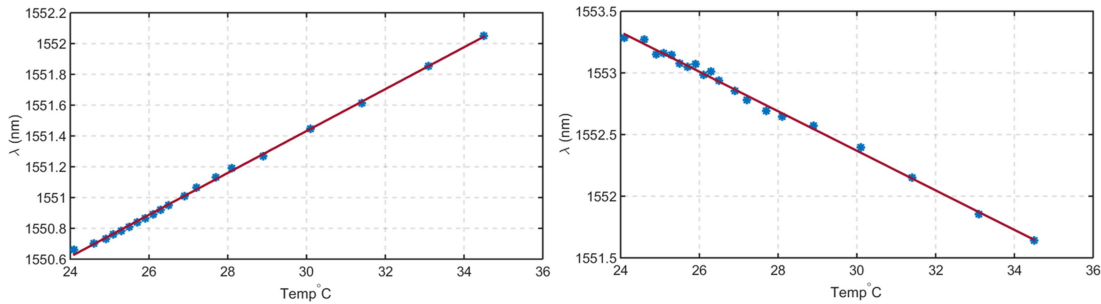
Fig. 14. Temperature sensitivity of the ring resonator (left) and the MZI sensor (right) with 90 nm slab partially exposed in air (with fit in solid red line).

simulated sensitivity percentage drop. The measured limit of detection (LOD) was defined from the 3-sigma deviation of the probability density function of the distribution of the measurements. The 3σ measured was around 123.6 pm and the resulting measured LOD was around 8.5×10^{-5} RIU.

VI. CONCLUSION

In order to realize a sensor with high levels of performance in terms of sensitivity and detection limit, a 1-cm long MZI partially exposed on a 90 nm slab was designed and fabricated. The expected sensitivity of the MZI sensor is ~2071 nm/RIU

at a wavelength of 1550 nm, and at a temperature of 300 K. A gas sensing experiment was performed on the partially exposed sensor switching N_2 and He gases alternatively, resulting in a measured sensitivity of ~1458 nm/RIU. Difference in measured and estimated sensitivities could be attributed to the fact that the effect of temperature was not accounted for in the simulation. A further reason is the 85° sidewall angle of the fabricated waveguide. The change in temperature in response to interchanging gases in the experiment was determined using a SiO_2-covered ring resonator, which was placed at the vicinity of the output of the MZI sensor. Changing the gas from He to N_2 has resulted in a temperature drop of around 0.27 K using

silicon's thermo-optic coefficient (1.86×10^{-4} K^{-1}). Further analysis was then conducted on the MZI sensor to study the effect of this temperature drop on the wavelength shift.

A separate temperature sensitivity test was conducted for both the partially exposed MZI sensor as well as the ring resonator. The temperature sensitivity of the ring resonator was measured to be 136 pm/°C and 166 pm/°C for the MZI sensor. It is apparent that the MZI sensor has a very low temperature dependence which is a fundamental requirement in all optical fluid sensors. Consequently, when taking the effect of the temperature drop on the partially exposed MZI sensor into consideration, the spectrum shifts towards the longer wavelengths resulting in an estimated sensitivity of around 1272 nm/RIU. The effect demonstrated that the small estimated drop in temperature has resulted only in a 12.75% decrease in the total sensitivity.

A suspended MZI sensor was also studied to further enhace the sensitivity by increasing the modal overlap with the measurand. The sensor had a predicted sensitivity as high as 5500 nm/RIU at a wavelength of 1550 nm which, as expected, is much higher than the sensitivty of the partially exposed MZI sensor. Fabrication errors were observed in SEM images of the suspended arm, including non-uniform undercut, presence of top cladding in different regions in the sensing arm and grating with Si fins much wider than intended in the design. Increasing the Si fin width increases the cladding refractive index which reduces the optical mode confinement and increases the propagation loss along the sensing arm as well as the bending loss. The aforementioned errors led to a considerable loss and thus no sensing experiment was conducted on the suspended MZI sensor.

REFERENCES

[1] V. Passaro, C. D. Tullio, B. Troia, M. L. Notte, G. Giannoccaro, and F. D. Leonardis, "Recent advances in integrated photonic sensors," *Sensors*, vol. 12, no. 11, pp. 15558–15598, 2012.

[2] K. Kim and T. E. Murphy, "Porous silicon integrated mach-zehnder interferometer waveguide for biological and chemical sensing," *Opt. Exp.*, vol. 21, no. 17, pp. 19488–19497, 2013.

[3] V. Passaro, F. Dell'Olio, B. Casamassima, and F. D. Leonardis, "Guided-wave optical biosensors," *Sensors*, vol. 7, no. 4, pp. 508–536, 2007.

[4] R. Chandrasekar, Z. J. Lapin, A. Nichols, R. Braun, and A. W. Fountain III, "Photonic integrated circuits for department of defense-relevant chemical and biological sensing applications: State-of-the-art and future outlooks," *Opt. Eng.*, vol. 58, no. 2, 2019, Art. no. 020901.

[5] Y.-n. Zhang, T. Zhou, B. Han, A. Zhang, and Y. Zhao, "Optical bio-chemical sensors based on whispering gallery mode resonators," *Nanoscale*, vol. 10, no. 29, pp. 13832–13856, 2018.

[6] I. M. White and X. Fan, "On the performance quantification of resonant refractive index sensors," *Opt. Exp.*, vol. 16, no. 2, pp. 1020–1028, 2008.

[7] J. G. Wangüemert-Pérez et al., "Evanescent field waveguide sensing with subwavelength grating structures in silicon-on-insulator," *Opt. Lett.*, vol. 39, no. 15, pp. 4442–4445, 2014.

[8] A. Densmore et al., "A silicon-on-insulator photonic wire based evanescent field sensor," *IEEE Photon. Technol. Lett.*, vol. 18, no. 23, pp. 2520–2522, Dec. 2006.

[9] X. Sun, D. Dai, L. Thylén, and L. Wosinski, "High-sensitivity liquid refractive-index sensor based on a mach-zehnder interferometer with a double-slot hybrid plasmonic waveguide," *Opt. Exp.*, vol. 23, no. 20, pp. 25688–25699, 2015.

[10] S.-H. Hsu and Y.-T. Huang, "A novel mach-zehnder interferometer based on dual-arrow structures for sensing applications," *J. Lightw. Technol.*, vol. 23, no. 12, pp. 4200–4206, Dec. 2005, Art. no. 4200.

[11] S. E. Yousuf et al., "Suspended microring resonator sensor using internal sub-wavelength grating," in *Proc. Adv. Photon.*, 2015, Paper SeS4C-4.

[12] J. T. Robinson, L. Chen, and M. Lipson, "On-chip gas detection in silicon optical microcavities," *Opt. Exp.*, vol. 16, no. 6, pp. 4296–4301, 2008.

[13] P. Dumais, C. L. Callender, J. P. Noad, and C. J. Ledderhof, "Integrated optical sensor using a liquid-core waveguide in a Mach-Zehnder interferometer," *Opt. Exp.*, vol. 16, no. 22, pp. 18164–18172, 2008.

[14] Q. Liu et al., "Highly sensitive Mach–Zehnder interferometer biosensor based on silicon nitride slot waveguide," *Sensors Actuators B: Chem.*, vol. 188, pp. 681–688, 2013.

[15] D. Yuan, Y. Dong, Y. Liu, and T. Li, "Mach-Zehnder interferometer biochemical sensor based on silicon-on-insulator rib waveguide with large cross section," *Sensors*, vol. 15, no. 9, pp. 21500–21517, 2015.

[16] M. Kitsara, K. Misiakos, I. Raptis, and E. Makarona, "Integrated optical frequency-resolved Mach-Zehnder interferometers for label-free affinity sensing," *Opt. Exp.*, vol. 18, no. 8, pp. 8193–8206, 2010.

[17] F. Prieto et al., "An integrated optical interferometric nanodevice based on silicon technology for biosensor applications," *Nanotechnology*, vol. 14, no. 8, 2003, Art. no. 907.

[18] R. Heideman and P. Lambeck, "Remote opto-chemical sensing with extreme sensitivity: Design, fabrication and performance of a pig-tailed integrated optical phase-modulated Mach–Zehnder interferometer system," *Sensors Actuators B: Chem.*, vol. 61, no. 1-3, pp. 100–127, 1999.

[19] B. Saleh and M. Teich, *Fundamentals of Photonics*. Hoboken, NJ, USA: Wiley, 2007.

[20] X. Jiang, Y. Chen, F. Yu, L. Tang, M. Li, and J.-J. He, "High-sensitivity optical biosensor based on cascaded Mach–Zehnder interferometer and ring resonator using vernier effect," *Opt. Lett.*, vol. 39, no. 22, pp. 6363–6366, 2014.

[21] G. N. Tsigaridas, "A study on refractive index sensors based on optical micro-ring resonators," *Photon. Sensors*, vol. 7, no. 3, pp. 217–225, 2017.

[22] Q. Shi, S. Sang, W. Zhang, P. Li, J. Hu, and G. Li, "Temperature sensor based on silicon microring," in *Proc. 13th IEEE Int. Conf. Nanotechnol.*, 2013, pp. 1224–1227.

[23] P. Xing and J. Viegas, "Broadband CMOS-compatible SOI temperature insensitive Mach-Zehnder interferometer," *Opt. Exp.*, vol. 23, no. 19, pp. 24098–24107, 2015.

[24] L. Chrostowski and M. Hochberg, *Silicon Photonics Design: From Devices to Systems*. Cambridge, U.K.: Cambridge Univ. Press, 2015.

[25] G. Cocorullo and I. Rendina, "Thermo-optical modulation at 1.5 mu m in silicon etalon," *Electron. Lett.*, vol. 28, no. 1, pp. 83–85, 1992.

[26] B. Guha, A. Gondarenko, and M. Lipson, "Minimizing temperature sensitivity of silicon Mach-Zehnder interferometers," *Opt. Exp.*, vol. 18, no. 3, pp. 1879–1887, 2010.

[27] M. Han and A. Wang, "Temperature compensation of optical microresonators using a surface layer with negative thermo-optic coefficient," *Opt. Lett.*, vol. 32, no. 13, pp. 1800–1802, 2007.

[28] J.-M. Lee, D.-J. Kim, H. Ahn, S.-H. Park, and G. Kim, "Temperature dependence of silicon nanophotonic ring resonator with a polymeric overlayer," *J. Lightw. Technol.*, vol. 25, no. 8, pp. 2236–2243, 2007.

[29] J.-M. Lee, D.-J. Kim, G.-H. Kim, O.-K. Kwon, K.-J. Kim, and G. Kim, "Controlling temperature dependence of silicon waveguide using slot structure," *Opt. Exp.*, vol. 16, no. 3, pp. 1645–1652, 2008.

[30] J. Teng et al., "Athermal SOI ring resonators by overlaying a polymer cladding on narrowed waveguides," in *Proc. 6th IEEE Int. Conf. Group IV Photon.*, 2009, pp. 77–79.

[31] B. Guha, J. Cardenas, and M. Lipson, "Athermal silicon microring resonators with titanium oxide cladding," *Opt. Exp.*, vol. 21, no. 22, pp. 26557–26563, 2013.

[32] J.-M. Lee, "Influence of titania cladding on SOI grating coupler and 5 μm-radius ring resonator," *Opt. Commun.*, vol. 338, pp. 101–105, 2015.

[33] M. Uenuma and T. Motooka, "Temperature-independent silicon wave-guide optical filter," *Opt. Lett.*, vol. 34, no. 5, pp. 599–601, 2009.

[34] S. Dwivedi, H. D'heer, and W. Bogaerts, "A compact all-silicon temperature insensitive filter for WDM and bio-sensing applications," *IEEE Photon. Technol. Lett.*, vol. 25, no. 22, pp. 2167–2170, Nov. 2013.

[35] T. Hiraki, H. Fukuda, K. Yamada, and T. Yamamoto, "Small sensitivity to temperature variations of Si-photonic Mach–Zehnder interferometer using Si and SiN waveguides," *Front. Mater.*, vol. 2, p. 26, 2015.

[36] R. J. Mathar, "Refractive index of humid air in the infrared: Model fits," *J. Opt. A: Pure Appl. Opt.*, vol. 9, no. 5, 2007, Art. no. 470.

[37] J.-M. P. Tournier and M. S. El-Genk, "Properties of helium, nitrogen and He-N2 binary gas mixtures," *J. Thermophysics Heat Transfer*, vol. 22, no. 3, pp. 442–456, 2008.

[38] J. Jágerská, H. Zhang, Z. Diao, N. Le Thomas, and R. Houdré, "Refractive index sensing with an air-slot photonic crystal nanocavity," *Opt. Lett.*, vol. 35, no. 15, pp. 2523–2525, 2010.

[39] K. Li et al., "l_n slot photonic crystal microcavity for refractive index gas sensing," *IEEE Photon. J.*, vol. 6, no. 5, pp. 1–9, Oct. 2014.

[40] F. Metehri, M. Y. Mahmoud, G. Bassou, E. Richalot, and T. Bourouina, "Stable optofluidic Fabry-Pérot resonator for liquid and gas sensing," *Sensors Actuators A: Phys.*, vol. 281, pp. 95–99, 2018.

[41] J. Tao et al., "A microfluidic-based Fabry-Pérot gas sensor," *Micromachines*, vol. 7, no. 3, p. 36, 2016.

[42] C. Liu, C. Sang, X. Wu, J. Cai, and J. Wang, "Grating double-slot micro-ring resonator for sensing," *Opt. Commun.*, vol. 499, 2021, Art. no. 127280.

[43] R. S. El Shamy, M. A. Swillam, M. M. ElRayany, A. Sultan, and X. Li, "Compact gas sensor using silicon-on-insulator loop-terminated Mach–Zehnder interferometer," in *Photonics*, vol. 9, no. 1. p. 8, 2022.